Lipid Magnetic Resonance Imaging Contrast Agent Interactions: A Spin-Labeling and a Multifrequency EPR Study

Tatyana I. Smirnova,* Alex I. Smirnov,* R. L. Belford, and R. B. Clarkson

Contribution from the Illinois EPR Research Center, Colleges of Veterinary Medicine and Medicine and Department of Chemistry, University of Illinois at Urbana–Champaign, Urbana, Illinois 61801

Abstract: The interactions of two lipophilic magnetic resonance imaging paramagnetic contrast agents, gadolinium complexes of 1,4,7,10-tetraazacyclododecane-N-(n-pentyl)-N',N'',N'''-triacetic acid (Gd-DOTAP) and 3,6,9-triaza-3,6,9-tris(carboxymethyl)-4-(4-ethoxybenzyl)undecandicarboxylic acid (Gd-EOB-DTPA), with model multilamellar liposomes prepared from 1,2-dimyristoyl-sn-glycero-3-phosphocholine (DMPC) were assessed in three sets of EPR experiments. The first two experiments were carried out with phospholipids selectively labeled with a series of spin-labeled doxyl stearic acids. By means of counting the collisions of molecular oxygen with a spin-labeled site, local oxygen permeability across the bilayer was measured with the contrast agents present and compared with control experiments in which contrast agents were absent. The maximum increase of $6.5 \pm 0.3\%$ for oxygen permeability at 20 mM Gd-DOTAP concentration was observed at 30.8 °C for the label located at the twelfth carbon position of the acyl chain. This result implied that Gd-DOTAP partitions within the DMPC bilayer, its preferred location being close to the bilayer center, and that the overall effect of Gd-DOTAP on the structural organization of the membrane is rather small. In contrast, no significant changes in local oxygen permeability were observed for Gd-EOB-DTPA. In the second set of spin-labeling experiments, the broadening of the spin-label spectra in the presence of Gd-DOTAP was measured as a function of position of the label across the bilayer. Again, maximum broadening was observed for the center of the bilayer, confirming the preferred location of this contrast agent. The third set of experiments utilized EPR spectroscopy of solutions of Gd^{3+} complexes at multiple high magnetic fields (corresponding microwave frequencies from 35 to 249 GHz). At these fields, Gd^{3+} serves as a useful probe to report on the microenvironment. Partitioning of Gd-DOTAP in DMPC liposomes resulted in partially resolved EPR spectra at 35 and 94.3 GHz. EPR experiments at multiple high fields (35, 94.3, and 249 GHz) show that the variation in spectral resolution observed across this frequency range arises from, first, line narrowing due to a decreased relative contribution of the zero field splitting (ZFS) in the spin Hamiltonian and, second, the shift of the resonance signal due to remaining ZFS effects. The frequency dependence of the apparent g-factor at multiple high magnetic fields as analyzed with third-order perturbation theory demonstrates a relationship between the observed shifts and the ZFS parameter. The analysis shows that Δ, the square root of the trace of the squared ZFS matrix, increases to 8.1 rad GHz when Gd-DOTAP partitions in the lipid phase of DMPC liposomes, up from 5.65 rad GHz for the aqueous phase. The high-field EPR method provides a direct measure of the populations of Gd complexes in various environments as well as an estimate of ZFS parameters in solutions.

Introduction

Contrast-enhanced magnetic resonance imaging (MRI) is a very effective technique for detecting and characterizing lesions, for identifying patho-physiological abnormalities, and for providing functional information. It has found wide application in clinical work and has become a powerful tool in research studies because of the rapid evolution in imaging techniques, improved methodology, and the development of efficient and specific contrast agents.

Rational development of new selective paramagnetic contrast agents (PCAs) requires a detailed understanding of their interactions with biological macromolecules and membranes and how these interactions affect the enhancement of the MRI image. Many parameters responsible for the image contrast may be affected by PCA–membrane interactions. These interactions may, for example, determine the retention time of a contrast agent in a tissue, modify the micro environment of the metal-binding site of the PCA, and/or affect the water exchange rate.

Little is known about the effect of contrast agents on phospholipid membranes. Binding or partitioning of PCAs within the lipids may affect the lipid–protein interactions and the heterogeneity of the lipid distribution in membranes. Interaction of contrast agents with lipids might be one of the factors that determine the transport mechanism of these complexes through the cell membranes. While it is speculated that some PCAs can cross the cellular membrane through the ion channels,[1] some intracellular PCAs exhibit sufficient lipophilicity to be delivered by a nonspecific mechanism (e.g., diffusion).

Here we describe how electron paramagnetic resonance (EPR) of Gd^{3+} complexes at multiple resonance frequencies, alone and in combination with spin-labeling methods, can provide information on the interactions of PCAs with model phospholipid bilayers.

(1) Weinmann, H.-J.; Bauer, H.; Frenzel, T.; Cries, H.; Schmitt-Willich, H.; Schuhmann-Giamperi, G.; Vogler, H. *Contrast-Enhanced Magnetic Resonance: Workshop Syllabus*, **1991**, Napa, CA, May 23–25.

One set of experiments undertaken in this study employs molecular oxygen to probe structural organization of the membranes exposed to lipophilic PCAs. Oxygen is more soluble in hydrocarbons than in aqueous media. Because of its small size, this molecule may enter any pockets transiently formed in the membrane and thus reflect even small changes and distortions in the membrane organization. By use of oxygen as a molecular probe, several membrane systems have been studied by EPR, including effects of cholesterol and alkyl chain unsaturation in phosphatidylcholine membranes,[2,3] molecular organization and dynamics in reconstituted protein-rich L-α-dimyristoylphosphatidylcholine membranes,[4] and effects of moderate ethanol concentrations on model phospholipid membranes.[5] The frequency of collision of a spin-labeled site with molecular oxygen as measured by EPR was used to demonstrate the presence and to determine the orientation of a helical segment in bacteriorhodopsin (mutants) with respect to the remainder of the protein[6] and to obtain topographical information on the sites in the membrane-bound protein.[7,8] EPR measurements of oxygen in biological systems are based on a spin label/spin probe approach: spin interactions with fast relaxing oxygen shorten the electronic T_1 and T_2 relaxation times of the probe. Effects of bimolecular collisions of a spin probe with an oxygen molecule or other spin-relaxing agents can be observed in pulsed saturation recovery EPR spectroscopy by comparison of the longitudinal relaxation rates, $1/T_1$, measured with and without spin-relaxing agents.[2-4] Variations in T_1 also can be measured in continuous wave (CW) EPR experiments from power saturation curves.[6-11] Dependence of a multiple-quantum EPR (MQEPR) signal upon the spin−lattice relaxation time T_1 of the spin probe has been shown to be another useful tool in spin-label oximetry.[12] In our study, we have applied an alternative CW EPR method based on accurate simulation of oxygen broadening effects by a convolution-type algorithm.[5,13] This method takes advantage of the high-sensitivity of CW EPR versus pulsed methods and does not require high microwave power, which can cause undesirable sample heating in power saturation experiments.

Another way to probe Gd^{3+} complexes in the vicinity of a biomolecule is to measure changes in the relaxation times of a spin label located at a specific site. The mechanism of spin−spin interaction between a metal complex and a spin probe, resulting in changes of relaxation time of the spin probe, is the subject of numerous discussions in the literature. Two types of interactions are responsible for changes in relaxation:

Heisenberg spin exchange and dipole−dipole interactions. Dipole−dipole interactions between the spin probe and the paramagnetic metal are generally dominant in solids, while Heisenberg exchange tends to be dominant in nonviscous liquids.[14-17] Usually, for high viscosities, the effect of the paramagnetic relaxer on the free radical signal is calculated assuming rigid-lattice-type dipolar interactions.[18] At very low viscosities, the dipolar interaction is considered to be completely averaged out by molecular motion and only exchange contributions to the line width are taken into account.

In biological systems that on the EPR time scale are neither liquid nor solid, dipolar and exchange interactions may be of comparable significance.[19] Conditions for collisions of paramagnetic metal ion complexes with free radicals, particularly orbital overlap for unpaired electrons and the diffusion rate, determine the relative effect of these interactions. Dipole−dipole interaction is effectively averaged out when translational diffusion is sufficiently fast compared with the second moment of dipolar interaction[14]

$$\tau_D^2 \ll \omega_d^2 \gg 1 \tag{1}$$

where τ_D is a characteristic time of the colliding species in the cage, ω_d^2 can be calculated as

$$\omega_d^2 = 5.1\gamma^2\hbar^2 S(S + 1)CR_{AB}^{-3} \tag{2}$$

and C is a concentration and R_{AB} is an average distance. For Gd^{3+} ($S = 7/2$), the product $S(S + 1)$ is unusually large while the exchange integral is smaller than for other ions because, for lanthanide ions, paramagnetic inner 4f orbitals are well shielded by outer 5s and 5p electrons.[19,20] Thus, a direct overlap of unpaired electron orbitals is unfavorable. Therefore, for most spin label−Gd^{3+} collisions, the dipolar mechanism ought to prevail over the spin exchange.[19] However, some of the dipolar contribution the EPR line shape still can be averaged out by spin flip-flops induced by spin−lattice relaxation and spin diffusion.[14,21] Unfortunately, to the best of the authors' knowledge, for the intermediate viscosity range there is no complete theory to describe the line shape of the spin-label signal broadened by a paramagnetic relaxer.[22] However, changes in the effective spin-label relaxation rate $1/T_1$ caused by dipolar and spin exchange interactions with a fast-relaxing paramagnetic metal ion have been shown to report reasonably accurate distances between the interacting spins, and the method has found some applications in studies of membranes and proteins.[10,23,24,] Changes in the relaxation rate of a nitroxide radical relative to that in the absence of a relaxer can be determined from power saturation experiments[19,25,26] or by saturation transfer electron spin resonance (STESR) spectroscopy.[23] The relaxation effects also alter to some extent the shape of CW EPR spectra.[19]

(2) Subczynski, W. K.; Hyde, J. S.; Kusumi, A. *Proc. Natl. Acad. Sci. U.S.A.* **1984**, *86*, 4474−4478.

(3) Subczynski, W. K.; Renk, G. E.; Crouch, R. K.; Hyde, J. S.; Kusumi, A. *Biochemistry* **1992**, *63*, 573−577.

(4) Ashikawa, I.; Yin, J.-J.; Subczynsli, W. K.; Kouyama, T.; Hyde, J. S.; Kusumi, A. *Biochemistry* **1994**, *33*, 4947−4952.

(5) Smirnov, A. I.;, Clarkson, R. B.; Belford R. L. *J. Magn. Reson. B.* **1996**, *111*, 149−157.

(6) Altenbach, C.; Marti, T.; Khorana, H. G.; Hubbell, W. L. *Science* **1990**, *248*, 1088−1092.

(7) Altenbach, C.; Flitsch, S. L.; Khorana, H. B.; Hubbell, W. L. *Biochemistry* **1989**, *28*, 7806−7812.

(8) Hubbell, W. L.; Altenbach, C. *Curr. Opin. Struct. Biol.* **1994**, *4*, 566−573.

(9) Subczynski, W. K.; Hyde, J. S. *Biochim. Biophys. Acta* **1981**, *643*, 283−291.

(10) Altenbach, C.; Greenhalgh, D. A.; Khorana, H. G.; Hubbell, W. L. *Proc. Natl. Acad. Sci. U.S.A.* **1994**, *91*, 1667−1671.

(11) Haas, D. A.; Mailer, C.; Robinson, B. H. *Biophys. J.* **1993**, *64*, 594−604.

(12) Mchaourab, H. S.; Hyde, J. S. *J. Magn. Reson. B* **1993**, *101*, 178−184.

(13) Smirnov, A. I.; Belford R. L. *J. Magn. Reson. A* **1995**, *113*, 65−73.

(14) Molin, Yu. N.; Salikhov, K. M.; Zamaraev, K. I. *Spin Exchange*; Springer-Verlag: Berlin, Germany, 1980; pp 133−146.

(15) Salikhov, K. M.; Doctorov, A. B.; Molin, Yu. N.; Zamaraev, K. I. *J. Magn. Reson.* **1971**, *5*, 189−205.

(16) Skubnevskaya, G. I.; Molin, Yu. N. *Kinet. Katal.* **1972**, *13*, 1383−1388.

(17) Eastman, M. P.; Kooser, R. G.; Das, M. R.; Freed, J. H. *J. Chem. Phys.* **1969**, *51*, 2690−2709.

(18) Leigh, J. S., Jr. *Chem. Phys.* **1970**, *52*, 2608−2612.

(19) Hyde, J. S.; Sarna, T. *J. Chem. Phys.* **1978**, *68*, 4439−4447.

(20) Hyde, J. S.; Swartz, H. M.; Antholine, W. E. In *Spin-Labeling II. Theory and Applications*; Berliner, L. J., Ed.; Academic Press: NY, 1979; pp 71−113.

(21) Maryasov, A. G.; Dzuba, S. A.; Salikhov, K. M. *J. Magn. Reson.* **1982**, *50*, 432−450.

Here we report the direct effects of a paramagnetic relaxer, a lipophilic Gd^{3+} complex, on line shapes of EPR spectra of phospholipid membranes labeled with a series of spin-labeled doxyl stearic acids. We have shown that, for low concentration of paramagnetic complexes, a one-parameter model, similar to the one we used to model oxygen broadening effects,[5,13] can be employed to simulate spin-labeled membrane spectra in the presence of the gadolinium complex. This method allows one to analyze CW EPR spectra for moderately small broadening effects and does not require high microwave power as in CW saturation experiments. The data on line broadening indicate unambiguously the distribution of the lipophilic Gd^{3+} complex across the lipid phase of the bilayer with a preferred location at its center.

Another way to observe interactions of Gd^{3+} complexes with biomolecules is directly from changes in their CW EPR Gd^{3+} spectra.[19,27] However, at conventional frequencies (X-band, 9.5 GHz), EPR signals from many Gd^{3+} complexes in aqueous solutions are very broad ($\gtrsim 400$ G) and are poorly modeled and understood. This, together with the low spectral resolution and low concentration sensitivity of X-band EPR of Gd^{3+} complexes, limits the usefulness of this method. Several studies have shown that the EPR line width of Gd^{3+} is magnetic field dependent and is primarily determined by the modulation of the zero field splitting (ZFS), which is induced by transient distortions of the symmetry of complexes.[28] Increasing the magnetic field decreases the relative contribution to the EPR line width arising from ZFS. This makes the line narrower and Lorentzian in shape,[29,30] thus simplifying the data analysis and improving the concentration sensitivity. Simplification of the line shape also allowed Powell and coauthors to estimate T_2 from solution CW EPR spectra and to evaluate the magnitude
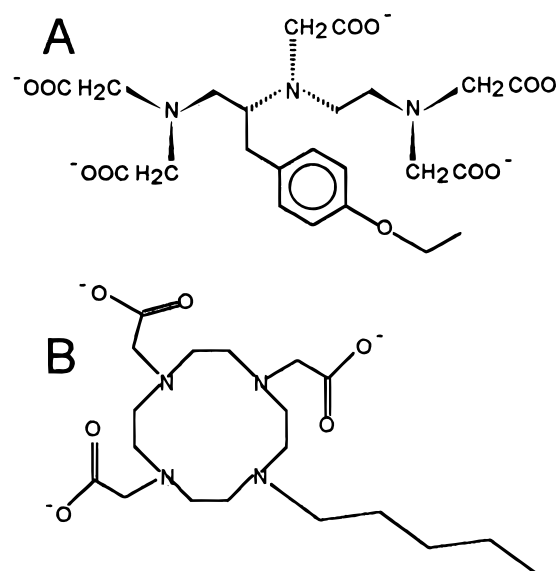
Figure 1. Chelates studied in this work: (A) EOB-DTPA = 3,6,9-triaza-3,6,9-tris(carboxymethyl)-4-(4-ethoxybenzyl)undecandicarbox-ylic acid and (B) DOTAP = 1,4,7,10-tetraazacyclododecane-*N*-(*n*-pentyl)-*N′*,*N″*,*N‴*-triacetic acid.

of ZFS for Gd^{3+} complexes from simultaneous fitting of multiple-field EPR line width data and results of nuclear magnetic resonance dispersion (NMRD) and ^{17}O NMR experiments.[30]

In this report, we demonstrate how measurements at 35 and 95 GHz EPR frequencies allowed us to differentiate the EPR signals arising from Gd^{3+} complexes distributed among different phases in a phospholipid bilayer and to quantitatively describe the partitioning. Complemented by 249 GHz EPR data, these experiments show that a decreased relative contribution of ZFS to the spin Hamiltonian at these high magnetic fields results not only in line narrowing but also in overall resonance shifts due to ZFS effects. By perturbation theory, we derive the relation between ZFS parameters of the complex and the average observed resonance shift of the solution spectra. Analysis of the frequency dependence of apparent *g*-factors for aqueous and lipid signals gives an estimate of the ZFS parameters of Gd^{3+} complex at physiologically relevant temperatures and shows that the ZFS increases when this PCA partitions within the membrane. This approach requires neither extensive sets of experimental data, like NMRD and ^{17}O NMR, nor global multiparameter fitting procedures.

Methods

Sample Preparation. The PCAs studied were gadolinium complexes of 1,4,7,10-tetraazacyclododecane-*N*-(*n*-pentyl)-*N′*,*N″*,*N‴*-triacetic acid (Gd-DOTAP) and 3,6,9-triaza-3,6,9-tris(carboxymethyl)-4-(4-ethoxybenzyl)undecandicarboxylic acid (Gd-EOB-DTPA). The chelate structure is shown in Figure 1. Contrast agents were provided by Schering AG, Germany, and used without further purification. Concentration of aqueous stock solution of each PCA was 100 mM.

Multilamellar liposomes were prepared from phospholipid DMPC (1,2-dimyristoyl-*sn*-glycero-3-phosphocholine; purchased from Avanti Polar Lipids, Alabaster, AL) by following the procedure given elsewhere;[31] however, no extrusion was performed. The final concentration of aqueous dispersion was 200 mg/mL. During the preparation, the membranes were labeled with one of the following: 5-doxylstearic acid (5-DS), 12-doxylstearic acid (12-DS), 16-doxylstearic acid (16-DS), cholestane spin label (CSL; all purchased from Aldrich, Milwau-

(22) In addition to the literature on spin-label−paramagnetic ion interactions that is cited throughout this paper, there is a body of theoretical work on electronic relaxation in radical pairs somewhat relevant to the subject at hand. However, these theories were developed either for normal liquids (Pedersen, J. B.; Freed, J. H. *J. Chem. Phys.* **1973**, *58*, 2746−2762; **1973**, *59*, 2869−2885. Monchick, L.; Adrian, F. J. *J. Chem. Phys.* **1978**, *68*, 4376−4383) or for the cases where diffusive motion can be neglected (Wang, Z.; Tang, J.; Norris, J. R. *J. Magn. Reson.* **1992**, *97*, 322−334). The above theories emphasize the spin exchange and neglect the dipole−dipole interaction, which dominates Gd^{3+}−spin-label interactions. Also, spin polarization effects, which are important for the relaxation of the radical pairs, are considered negligible for the fast-averaging paramagnetic metal ion−spin-label interactions. Other relevant literature concerns EPR of biradicals (for a review see, e.g., Luckhurst, G. R. In *Spin Labeling. Theory and Applications*; Berliner, L. J., Ed.; Academic Press: NY, 1976; pp 133−183) and double-spin-labeled proteins. Some labels can be rigidly attached to proteins and electron−electron dipolar coupling can be clearly resolved from CW EPR spectra, especially at high magnetic fields (Hustedt, E. J.; Smirnov, A. I.; Laub, C. F.; Cobb, C. E.; Beth, A. H. *Biophys. J.* **1997**, *74*, 1861−1877). In contrast, rotational motion of flexibly attached labels with respect to the protein backbone causes in some averaging of dipole−dipole interactions. This averaging results in a homogeneous broadening across the EPR spectrum, which was modeled by convolution with a Lorentzian function and interpreted using Abraham's results (Mchaourab, H. S.; Oh, K. J.; Fang, C. J.; Hubbel, W. L. *Biochemistry* **1997**, *36*, 307−316).

(23) Páli, T.; Bartucci, R.; Horváth, L. I.; Marsh D. *Biophys. J.* **1992**, *61*, 1595−1602.

(24) Likhtenshtein, G. I. *Biophysical Labeling Methods in Molecular Biology*; Cambridge University Press: NY, 1993; pp 70−71.

(25) Kulikov, A. V.; Likhtenshtein, G. I. *Biophysics* **1974**, *19*, 424−428.

(26) Likhtenshtein, G. I. *Pure Appl. Chem.* **1990**, *62*, 281−288.

(27) Reuben, J. J. *J. Phys. Chem.* **1971**, *75*, 3164−3167.

(28) Abragam, A.; Bleaney, B. *Electron Paramagnetic Resonance of Transition Ions*; Dover Publications: NY, 1986; pp 133−216.

(29) Powell, D. H.; Merbach, A. E.; González, G.; Brücher, E.; Micskei, K.; Ottaviani, M. F.; Köhler, K.; von Zelewsky, A.; Grinberg, O. Ya.; Lebedev, Ya. S. *Helv. Chim. Acta* **1993**, *76*, 2129−2146.

(30) Powell, D. H.; Ni Dhubhghaill, O. M.; Pubanz, D.; Helm, L.; Lebedev, Ya. S.; Schlaepfer, W.; Merbach, A. E. *J. Am. Chem. Soc.* **1996**, *118*, 9333−9346.

(31) Smirnov, A. I.; Smirnova, T. I.; Morse, P. D., II *Biophys. J.* **1995**, *68*, 2350−2360.

kee, WI) 4-(*N,N*-dimethyl-*N*-(2-hydroxyethyl))ammonium-2,2,6,6-tetramethylpiperidine-1-oxyl, chloride (tempo-choline), and 4-(octadecanoyloxy)-2,2,6,6-tetramethylpiperidine-1-oxyl (tempo-stearate; purchased from Molecular Probes, Inc., Eugene, OR). The probe-to-lipid ratio was 1:100. A rather high pH, 9.5, was chosen to ensure that all carboxyl groups of the doxyl probes are ionized in the DMPC membrane (1.1 M borate−potassium hydroxide buffer at pH = 9.5[2,32,33]). The same pH was maintained upon addition of Gd^{3+} complexes to avoid changing the protonation state of the carboxyl groups of the doxyl probes.

For model experiments, Gd-DOTAP was dissolved in oleic acid (Sigma, St. Louis, MO) by vortexing at room temperature equal amounts of oleic acid and 10 mM Gd-DOTAP aqueous solutions at either pH = 5.6 or 9.5 and then separating the two phases by centrifugation.

X-Band Measurements. Spin-labeled phospholipid samples were drawn into a gas-permeable poly(tetrafluoroethylene) (TFE) capillary (0.81 mm i.d., 0.86 mm o.d.; Zeus Industrial Products, Raritan, NJ), the ends were closed by folding, and the capillary was placed inside a quartz tube (3 mm i.d.) open at both ends. The tube was fixed inside the variable-temperature dewar of the X-band EPR resonator. Samples were deoxygenated in the EPR cavity by continuous flow of nitrogen gas around the gas-permeable capillary-containing sample.[34] For measuring local oxygen permeability in the phospholipid bilayer, the gas flow was consequently switched to oxygen. A Varian (Palo Alto, CA) Century Series E-112 X-band spectrometer was equipped with a Varian TE$_{102}$ cavity and a Varian temperature controller. Temperature was measured with a miniature T-type thermocouple fixed next to the sample capillary and an Omega Engineering (Stamford, CT) 670/680 microprocessor-based thermocouple meter. Stabilization of the gas flow in addition to fixed positions of sample and thermocouple sensor in the dewar insert significantly improved temperature stability of the sample. In addition, before the experiments, we allowed at least 1 h for the system to stabilize. Temperature was stable and repeatable within ±0.1 °C from measurement to measurement. Systematic errors of temperature measurements were within ±0.4 °C. Inevitable temperature gradients existing in the dewar insert[35] resulted in additional ±0.5 °C error between the sample and the sensor. The data were corrected for these systematic errors.

Q-Band Measurements. A Varian Century Series E-115 Q-band spectrometer was equipped with a cylindrical Varian TE$_{011}$ cavity. Fused quartz capillaries (0.30 mm i.d., 0.40 mm i.d., VitroCom, Inc., Mountain Lakes, NJ) were used to measure EPR from aqueous samples at room temperature. The magnetic field was calibrated with a tracking NMR Gaussmeter (Varian model 92980102P). The microwave frequency was measured by an EIP-578 in-line microwave frequency counter (EIP Microwave, Inc., San Jose, CA). An aqueous solution of perdeuterated Tempone (4-oxo-2,2,6,6-tetramethyl-1-piperidinyloxy, Isotec, Inc., Miamisburg, OH) was used as a secondary *g*-factor standard.

Measurements at 94 and 249 GHz. The W-band (94 GHz) spectrometer constructed at the University of Illinois EPR Research Center is described elsewhere.[36] For the experiment described here, a second spectrometer was used that differs from the previous configuration[31,36,37] in having an Oxford (Oxford Instruments, Inc., Concord, MA) custom-built 7 T superconductive magnet outfitted with a water-cooled coaxial sweep coil (University of Illinois). This sweep coil provided a variable scan/offset up to ±550 G from the main field under digital (15 bits resolution) computer control. The scan and the center of magnetic field were calibrated with a Metrolab precision NMR

teslameter PT 2025 (GMW Associates, Redwood City, CA). The microwave frequency was measured with a source-locking microwave counter (Model 578, EIP Microwave Inc., San Jose, CA). The cavity was a cylindrical type TE$_{01n}$ (*n* = 2, 3 depending upon tuning) made of a gold foil (0.025 mm thick, purchased from Alfa Aesar, Ward Hill, MA) lining a quartz support cylinder (Wilmad Glass, Buena, NJ). The quality factor of the unloaded cavity is 4000. The variable-temperature system was outfitted with a modified constant-flow CF1200 cryostat, an AutoGFS transfer line, and an ITC-4 digital temperature controller (all supplied by Oxford Instruments, Inc.). The temperature was considered stable if the readings of both thermometers were the same within the measurement accuracy, ±0.1 °C. Stability of the resonance frequency of the cavity (±25 kHz) during the measurement was also an indication of temperature stability. Samples were drawn into quartz capillaries with i.d. = 0.15 mm and o.d. = 0.25 mm (VitroCom, Inc.) and sealed with Critoseal (Fisher Scientific, Pittsburgh, PA).

The 249 GHz experiments were carried out in the laboratory of Prof. Freed (Baker Laboratory of Chemistry, Cornell University, Ithaca, NY) with an instrument built in that laboratory and described elsewhere.[38]

Spectral Simulations. To extract line broadening induced by the presence of a paramagnetic relaxer (e.g., molecular oxygen) from continuous-wave EPR spectra, inhomogeneously broadened EPR spectra of spin-labeled doxyl stearic acids were simulated under a one-line-width-parameter model[5,13,39]

$$F(B) = \int_{-\infty}^{+\infty} F_0(B') m(B - B') \, dB' \tag{3}$$

where $F_0(B)$ is the spectrum taken in the absence and $F(B)$ in the presence of a relaxer, and $m(B)$ is the Lorentzian broadening measured as $\delta(\Delta B^L_{p-p})$. Since the oxygen−spin probe interaction is dominated by the Heisenberg spin exchange (the effect of dipole−dipole interaction in most cases being negligible[40]), the oxygen permeability coefficient $P(O_2)$ (determined as a product of oxygen diffusion and solubility coefficients) is proportional to $\delta(\Delta B^L_{p-p})$

$$P(O_2) = \frac{\sqrt{3}\gamma\delta(\Delta B^L_{P-P})}{8\pi Rc} \tag{4}$$

where R is the collision distance and c is the probability that the spin exchange occurs. The product (Rc) for doxyl stearic acid probes is not accurately known, but it is usually assumed that its value (∼2 Å)[41] does not vary with position of the nitroxide moiety.[2,41] We have previously shown that model eqs 3 and 4 are applicable to the measurement of oxygen permeability coefficients from nitroxides in the fast motion limit[13,39] as well as from doxyl stearic acid and cholestane membrane probes in phospholipid bilayers at temperatures corresponding to ripple and fluid bilayer phases.[5]

The model does not require accurate modeling of anisotropically averaged doxyl stearic acids' EPR spectra from the membranes; all contributions to the line shape arising from modulation of magnetic matrixes by rotational motion as well as those due to inhomogeneous width are automatically accounted for by eq 3.

To obtain low-temperature ZFS parameters, the rigid-limit 95 GHz EPR spectra were simulated with program PIP,[42] a modified version of QPOW program.[43]

(32) Kusumi, A.; Subczynski, W. K.; Hyde, J. S. *Proc. Natl. Acad. Sci. U.S.A.* **1982**, *79*, 1854.
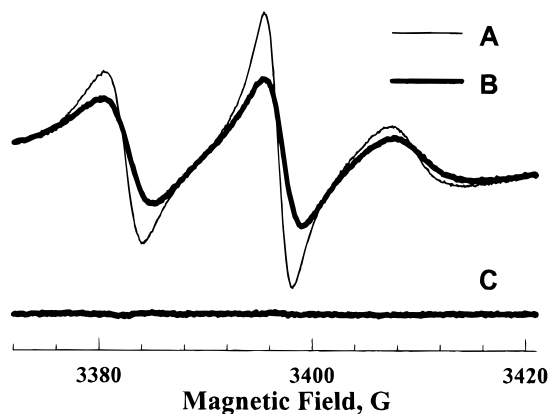
(33) Träube, H.; Eibl, H. *Proc. Natl. Acad. Sci. U.S.A.* **1974**, *71*, 214−219.

(34) Smirnov, A. I.; Norby, S.-W.; Weyhenmeyer, J. A.; Clarkson, R. B. *Biochim. Biophys. Acta* **1994**, *1200*, 205−214.

(35) Morse, P. D., II; Magin, R. L.; Swartz, H. M. *Rev. Sci. Instrum.* **1985**, *6*, 94−96.

(36) Wang, W.; Belford, R. L.; Clarkson, R. B.; Davis, R. B.; Forrer, R. B.; Nilges, M. J.; Timken, M. D.; Watczak, T.; Thurnauer, M. C.; Norris, J. R.; Morris, A. L.; Zwang, Y. *Appl. Magn. Reson.* **1994**, *6*, 195−215.

(37) Smirnova, T. I.; Smirnov, A. I.; Clarkson, R. B.; Belford, R. L. *J. Phys. Chem.* **1995**, *99*, 9008−9016.

(38) Lynch, W. B.; Earle, K. A.; Freed, J. H. *Rev. Sci. Instrum.* **1988**, *59*, 1345−1351. Barnes, J. P.; Freed, J. H. *Rev. Sci. Instrum.* **1997**, *68*, 2838−2846.

(39) Smirnova, T. I.; Smirnov, A. I.; Clarkson, R. B.; Belford, R. L. *Magn. Reson. Med.* **1995**, *33*, 801−810.

(40) Hyde, J. S.; Subczynski, W. K. In *Biological Magnetic Reson*ance; Berliner, L. J., Reuben, J., Eds.; Plenum Press: NY, 1989; Vol. 8, pp 399−425.

(41) Windrem, D. A.; Plachy, W. Z. *Biochim. Biophys. Acta* **1980**, *600*, 655−665.

(42) Nilges, M. J., Illinois EPR Research Center (IERC), University of Illinois. To obtain the software at the IERC's ftp site use the following steps: 1. Ftp ierc.scs.uiuc.edu. 2. At the login prompt, type *anonymous*. 3. Enter your e-mail address as a password. 4. Type *get README.1st* to read what files are on the site and where they are located. 5. Change directory to the desired directory with the command *cd directory_name*. 6. Issue the command *get filename* to get the desired file.
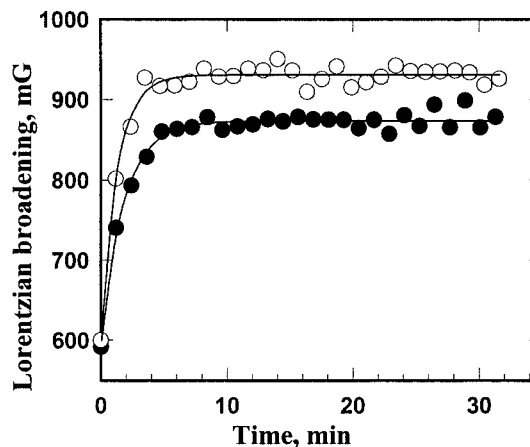
Figure 2. Experimental X-band spectra from 12-DS in DMPC aqueous dispersion (pH = 9.5) in the presence of 20 mM Gd-DOTAP at 30.8 °C equilibrated with nitrogen (A) and subsequently with oxygen (B). Spectrum B was fitted to a model of additional Lorentzian broadening as described in the text. The best-fit Lorentzian broadening was $\delta(\Delta B^L_{p-p}) = 0.948 \pm 0.005$ G. Spectrum C is the residual, the difference between the experimental and the simulated spectrum.

Results and Discussion

Spin-Labeling X-Band EPR Experiments. In the first set of experiments, effects of two gadolinium complexes on local structure and dynamics of DMPC membrane were assessed by spin-labeling methods and CW X-band EPR. A series of membrane spin labels was incorporated into the bilayer at various depths. Changes in local chain motion of the phospholipids and ordering of the probes can be monitored by measuring the splittings and line widths of characteristic EPR spectral features (e.g., parameters $A'_{\parallel}$ and $A'_{\perp}$ for probes exhibiting a substantial degree of ordering[44]) and enhancing this information by computer simulations.[45,46] In our experiments, we observed that the characteristic splitting of EPR spectra from spin-labeled fatty acids was unaffected by the presence of lipophilic PCAs in concentrations up to 10 mM; however, for several probes, some broadening of the spectral features was observed. This indicates that the structural changes in membrane organization with the presence of lipophilic PCAs are rather small and that the broadening of the nitroxide spectrum is more likely caused by spin–spin interactions between PCA and spin label.

The use of molecular oxygen in combination with the spin-labeling CW EPR method appears to be a more sensitive technique to probe changes in the membrane structural organization than CW EPR of spin labels alone.[5] We used this method to determine whether there is any perturbation of the membrane structure induced by two intracellular MRI contrast agents (Gd-DOTAP and Gd-EOB-DTPA). A maximum in this perturbation would indicate a preferred location of the Gd^{3+} complexes in the bilayer.

Application of the oxygen permeability CW EPR method to the PCA/DMPC system is demonstrated in Figures 2−4. Figure 2 shows experimental X-band spectra from 12-DS in DMPC aqueous dispersion, in the presence of 20 mM Gd-DOTAP at 30.8 °C, equilibrated with nitrogen (A) and subsequently with oxygen (B). A model of additional Lorentzian broadening (see

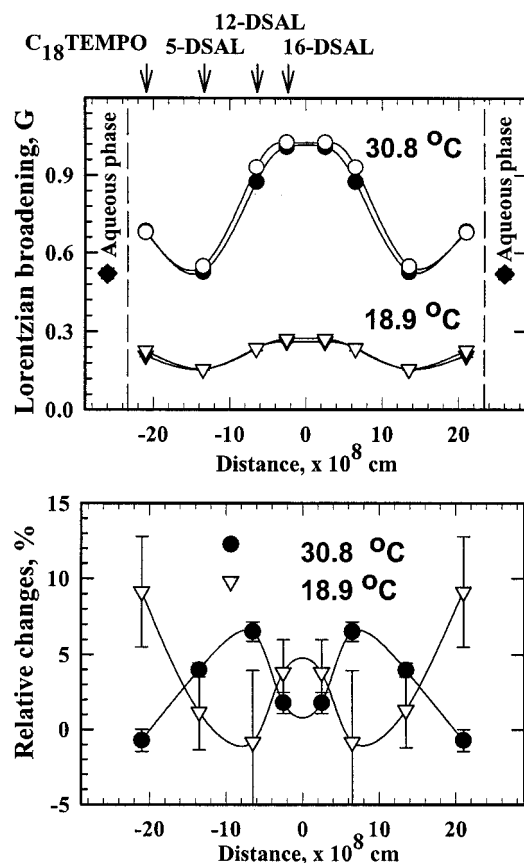(43) Nilges, M. J. Ph.D. Thesis, University of Illinois, 1979.
(44) Gaffney, B. J. In *Spin-Labeling. Theory and Applications*; Berliner, L. J., Ed.; Academic Press: NY, 1976; pp 567−571.
(45) Schneider, D. J.; Freed, J. H. In *Biological Magnetic Resonance*; Berliner, L. J., Reuben, J., Eds.; Plenum Press: NY, 1989; Vol. 8, pp 1−76.
(46) Budil, D. E.; Lee, S.; Saxena, S.; Freed, J. H. *J. Magn. Reson. A* **1996**, *120*, 155−189.

Figure 3. Kinetics of equilibration of DMPC membrane (pH = 9.5) with oxygen as measured by 12-DS fitted to exponential functions (shown as solid lines). Open circles correspond to a sample containing 20 mM of Gd-DOTAP (average broadening at equilibrium $\delta(\Delta B^L_{p-p})$ = 0.931 ± 0.002 G); filled circles correspond to the control ($\delta(\Delta B^L_{p-p})$ = 0.874 ± 0.002 G).

eq 3) applied to fit the spectra was found to describe the oxygen broadening extremely well. That the fit matches the experimental spectrum almost perfectly (residual, difference between the experimental and the simulated spectrum, shown in Figure 2C) confirms the utility of the fitting model given by eq 3 for this system. Lorentzian broadening of this spectrum by molecular oxygen was measured; $\delta(\Delta B^L_{p-p})$ = 0.948 ± 0.005 G. To increase the accuracy and to ensure that the sample is in equilibrium with the surrounding gas, we collected sequential spectra to follow ΔB^L_{p-p} kinetics after the gas was switched from nitrogen to oxygen. This kinetics mainly reflects oxygen diffusion through the TFE walls into a limited volume of the capillary containing the membrane sample. For our experimental conditions, the ratio of the amount of oxygen soluble in the capillary walls to that inside the capillary (measured at equilibrium) is small and the kinetics is well approximated by a single-exponential term when approaching the equilibrium (for more details see ref 47). Figure 3 shows an example of such kinetics for the DMPC membrane labeled with 12-DS. Equilibration curves were fitted to first-order kinetics to measure $\delta(\Delta B^L_{p-p})$ at equilibrium. Open circles correspond to the sample containing 20 mM of Gd-DOTAP (average broadening at equilibrium $\delta(\Delta B^L_{p-p})$ = 0.931 ± 0.002 G); filled circles correspond to the control ($\delta(\Delta B^L_{p-p})$ =0.874 ± 0.002 G). Thus, in the presence of 20 mM Gd-DOTAP, the oxygen permeability of the DMPC bilayer measurably increases (by 6.5 ± 0.3%) as was observed with a nitroxide label which was located at the twelfth carbon position of the acyl chain of the fatty acid molecule. Figure 4 summarizes results of the oxygen permeability experiments for several locations of the nitroxide label within the membranes at temperatures above (30.8 °C) and below (18.9 °C) the main phase transition of DMPC which occurs at $T \approx 23$ °C. Parameter $\delta(\Delta B^L_{p-p})$ for the aqueous phase was measured with nitroxide tempo-choline. The approximate location of the nitroxide moiety of spin-labeled stearic acids in the DMPC membrane is given as in the literature.[41,48] The oxygen profile for a control sample (no PCA) is in general agreement with literature data.[2,5,41] The lower plot on Figure 4 shows relative changes in the local oxygen membrane perme-

(47) Smirnov, A. I.; Norby, S.-W.; Weyhenmeyer, J. A.; Clarkson, R. B. *Biochim. Biophys. Acta* **1993**, *1200*, 205−214.
(48) Schreier-Muccillo, S.; Marsh, D.; Smith, I. P. C. *Arch. Biochem. Biophys.* **1976**, *172*, 1−11.

Figure 4. Upper plot: profiles of Lorentzian oxygen broadening parameter $\delta(\Delta B^L_{p-p})$ across the DMPC membrane for two temperatures, below (18.9 °C) and above (30.8 °C) the main phase transition. Open symbols correspond to a sample containing 20 mM of Gd-DOTAP (pH = 9.5); filled symbols correspond to the control. Approximate location of spin labels in the membrane is shown by arrows (DSAL = doxylstearic acid label). Parameter $\delta(\Delta B^L_{p-p})$ for the aqueous phase was measured with the nitroxide tempo-choline and is shown as a diamond. Variation of this parameter with the temperature was within the error bars shown. Variations of $\delta(\Delta B^L_{p-p})$ for locations are within the size of the symbols. Approximate location of aqueous phase given by dashed lines. Lower plot: relative changes in local oxygen permeability across the DMPC membrane in the presence of 20 mM of Gd-DOTAP (pH = 9.5) at 18.9 °C (open triangles) and at 30.8 °C (filled circles) calculated from data shown in upper plot.

ability in the presence of 20 mM Gd-DOTAP. At 18.9 °C (DMPC membrane in the ripple phase), local oxygen permeability is much smaller than when the membrane is in the fluid bilayer phase (30.8 °C; Figure 4, upper plot), and the errors for the 18.9 °C data are relatively large (Figure 4, lower plot). At 18.9 °C (temperature below the main phase transition of the membrane), the relative effect is maximal at the polar head region and at the bilayer center, while above the phase transition (30.8 °C), the largest increase was observed for the nitroxide moiety at the twelfth carbon position of the acyl chain. This result is not unexpected because Gd-DOTAP has a lipophilic pentane "tail" which might cause some partitioning of the agent into the bilayer lipid phase. While located between the acyl chains, this PCA could create some disorder, which would increase the local oxygen permeability. We speculate that magnitude of this distortion is determined by not only the distribution of Gd-DOTAP within the bilayer but also the local packing/order parameter of the phospholipids. If so, then the observed decrease in the relative effect from 12-DS to 16-DS can be explained by a very little ordering of the lipid chains at

the bilayer center (sixteenth carbon position) when the membrane is in the fluid bilayer phase (i.e., Gd-DOTAP cannot cause any more disorder).

Overall, the oxygen permeability experiment indicates that Gd-DOTAP might be partitioning within the DMPC membrane. Relative changes in the local oxygen permeability, measured with a better accuracy at 30.8 °C (fluid bilayer phase) than at 18.9 °C (ripple phase), are maximal at the twelfth carbon position of the acyl chain, indicating that there is a preferred location for the Gd-DOTAP close to the bilayer center. At both temperatures, the effect of Gd-DOTAP on the oxygen permeability was quite moderate. For example, at 30.8 °C (fluid bilayer phase) the increase was 6.5 ± 0.3% as measured by 12-DS. Thus, even at concentrations higher than average levels expected in medical applications (clinical doses for PCAs are usually from 50 to 100 μmol per kg body weight), the overall effect of the Gd-DOTAP on the membrane oxygen permeability properties is quite moderate.

In contrast, the same measurements carried out with Gd-EOB-DTPA showed extremely small, if any, effects of the agent on local oxygen permeability. For example, 20 mM of Gd-EOB-DTPA increased the local permeability as measured by 12-DS by only 1.0 ± 0.3%. Comparison of changes in oxygen profiles induced by these two Gd complexes shows that distortions in local order created by partitioning of the Gd-EOB-DTPA in the phospholipid membrane is negligibly small compared to that of Gd-DOTAP. The reason might be a very low partitioning coefficient of this PCA into the membrane lipid phase.

EPR spectra of deoxygenated DMPC samples labeled with 12- and 16-DS showed some line broadening when Gd-DOTAP was added, and this served as another indication of the paramagnetic relaxer's presence within the bilayer center. The spectra collected for deoxygenated samples were further analyzed for these broadening effects, which are caused by spin−spin interactions between the PCA molecules and the nitroxide labels.

Two magnetic interactions, Heisenberg spin exchange and dipole−dipole coupling, could cause Gd-DOTAP to broaden the CW EPR spin-label spectrum. Heisenberg exchange with a paramagnetic ion shortens the transverse relaxation time T_2 of the label and contributes to the line width as an additional Lorentzian broadening.[14] Dipole−dipole interactions, which seems to be dominant for Gd−spin label interactions, also contribute to the line width ΔB; an explicit expression for the line width is a subject of discussion in the literature.[49] Many authors have used the results of Abragam[50] for calculating dipolar broadening effects within the Brownian diffusion model

$$\Delta\left(\frac{1}{T_1}\right) = \frac{64\pi^2}{15}\frac{a_1 a_2}{(a_1 + a_2)^2} N_{ion}\gamma_e^2\hbar^2 S_m(S_m + 1)\gamma_m^2\frac{\eta}{kT} \quad (5)$$

where a_1 and a_2 are the radii of the colliding species and the rest of the notation is as defined by Abragam.[50] Dipolar contributions to the longitudinal and the transverse relaxation rates of spin label are usually assumed to be equal $\Delta(1/T_1) = \Delta(1/T_2)$. Freed and co-workers have presented similar theoretical results.[51] Freed's group has developed a more realistic treatment for diffusion of the interacting particles, including, e.g., jumps of a finite size.[52,53] All of these theoretical treatments give a Lorentzian shape for the dipolar broadening.

(49) Eaton, S. S.; Eaton, G. R. *Coord. Chem. Rev.* **1978**, *26*, 207−262.
(50) Abragam, A. *The Principles of Nuclear Magnetism*; Oxford University Press: London, 1961; pp 289−304.
(51) Eastman, M. P.; Kooser, R. G.; Das, M. R.; Freed, J. H. *J. Chem. Phys.* **1969**, *51*, 2690−2709.
(52) Hwang, L.-P.; Freed, J. H. *J. Chem. Phys.* **1975**, *63*, 4017−4025.
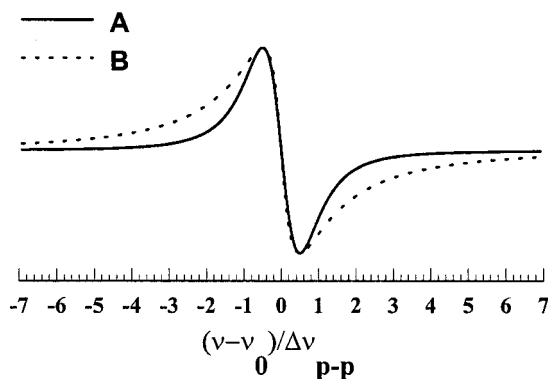
Figure 5. Comparison between a Lorentzian line shape (A) and a dipolar profile (B) given by a Fourier transform of eq 6 for the same peak-to-peak width and amplitude of the first derivative spectra.

Figure 6. Experimental X-band spectra from a cholestane spin label (CSL) in nitrogen-equilibrated DMPC aqueous dispersion at 30.8 °C (A) and in the presence of 10 mM Gd-DOTAP, pH = 9.5 (B). The spectrum B is fitted to an additional Lorentzian-broadening model of as described in the text. The best-fit Lorentzian broadening is $\delta(\Delta B^{L}_{p-p})$ = 0.095 ± 0.005 G. Spectrum C is the residual, the difference between the experimental and the simulated spectrum.

In another theoretical study, Salikhov and co-workers have calculated the free induction decay (FID) for a system of $S = {}^{1}/{}_{2}$ spins with anisotropic g-factors interacting via dipolar coupling.[21] A model of magnetically diluted solids in which dipolar broadening is much less than inhomogeneous line width thus allowing an adiabatic approximation for the dipole−dipole interaction was considered. It has been shown that in the high-temperature limit, when dipole−dipole interaction is modulated by random spin flip-flops, the spin polarization effects are negligible, and the FID, $\nu_{FID}(t)$, is no longer a simple exponential, rather is taken the form
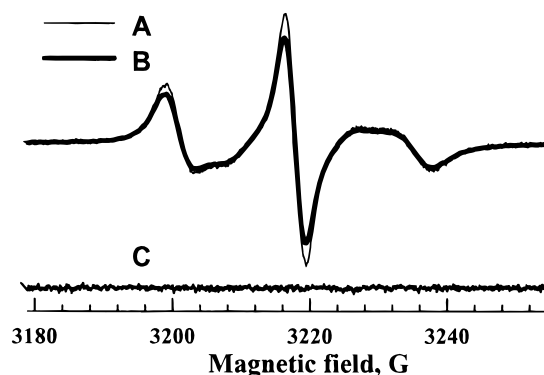
$$\nu_{FID}(t) \approx \exp(-a(t)^{1/2}) \qquad (6)$$

where

$$a = \frac{8\pi^{3/2}}{3^{5/2}}\langle g^2 \rangle \beta^2 \hbar^{-1} C(T_1)^{1/2} \qquad (7)$$

$\langle g^2 \rangle$ is a weighted g-factor for the two interacting species,[21] C is spin concentration, and T_1 is the spin−lattice relaxation time. The corresponding CW spectrum $\mathbf{V}(\omega)$ is given by a Fourier transform and is not Lorentzian; while the central part is slightly sharper than the Lorentzian for the same peak-to-peak line width ΔB_{p-p}, the wings vanish less rapidly (see Figure 5 for comparison of first-derivative spectra with the same peak-to-peak line width and amplitude). As a result, dipolar broadening as given by eq 6 decreases the peak-to-peak intensity of the CW spin-label spectrum by adding very broad wings with only a little broadening of the central part. Although this model does not consider translational diffusion, it does include averaging of dipolar interaction by mutual spin reorientations, which are very likely to occur in our system.

Under a model of additional broadening (eq 3), we have simulated effects of Gd-DOTAP on the EPR spectra of spin-labeled DMPC membrane. For this model to apply, addition of a paramagnetic relaxer to a spin-labeled phospholipid bilayer should not measurably affect the motion of the spin probe. This condition was satisfied, as evidenced by the splittings between characteristic turning points of the spin-label spectra being the same within the experimental accuracy in absence and presence of the Gd^{3+} complexes studied.

Initially, a Lorentzian broadening model was used to simulate the broadening effects caused by 10 mM Gd-DOTAP at 30.8 and 18.9 °C that correspond to ripple and fluid bilayer phases, respectively. Figure 6 demonstrates results of spectral simula-

tions under eq 3 for CSL spin-labeled DMPC membrane in a fluid bilayer phase (30.8 °C). The Lorentzian broadening model describes the spectrum quite well; the residual of the fit (difference between simulated and experimental spectrum) shows no significant deviations between experiment and fit. The absence of these deviations also indicates that at 10 mM Gd-DOTAP, the changes in $F_0(B)$ (eq 3), which is determined by rotational motion of the probe, were insignificant on the EPR scale; thus, the CSL motion was unaffected.

For the CSL probe at 30.8 °C, the extracted peak-to-peak Lorentzian broadening at 10 mM Gd-DOTAP was 99 ± 5 mG, which is small compared with the width of characteristic spectral features ($\Delta B \gtrsim 1$ G). Therefore, one expects the fit to be relatively insensitive to the broadening functions chosen (e.g., broadening function given by Fourier transform of eq 6 fits equally well). For other faster-rotating spin probes (e.g., 12- and 16-DS), we found the same good agreement of the broadening of CW EPR spectra with the Lorentzian model providing the concentration of the Gd-DOTAP did not exceed 10 mM. At higher (20 mM) concentration ($T = 30.8$ °C), the broadening increased and somewhat higher residual norm was observed. Particularly, the wings of the spectra appeared slightly broader than the best fit with Lorentzian as a broadening function in eq 3.

The central 10 G portions of 16-DS EPR spectra taken at 30.8 °C were analyzed further by applying Lorentzian and non-Lorentzian, $V(\omega)$, broadening functions ($V(\omega)$ being a Fourier transform of ν_{FID}, eq 6). The $V(\omega)$ function was chosen to model averaging of dipole−dipole interaction by random spin reorientations. Simulations were carried out as follows. Initially, the central 10 G portion of a 16-DS spectrum taken in absence of Gd-DOTAP was modeled as a Gaussian−Lorentzian convolution. Compared with analysis of membrane spin-label EPR spectra given in ref 54, a better accuracy was achieved by calculating the Gaussian−Lorentzian convolution digitally by Fourier transform and by including a single carbon-13 satellite rather than using a Gaussian−Lorentzian sum approximation. The linear baseline term was set to zero and was not adjusted during all simulations. The fit (Table 1, fit 1) was exceptionally good. The residual norm was defined as where σ_i was assumed

$$\chi^2 = \frac{1}{N-M}\sum_{i=1}^{N}\frac{[F_i - F(B_i)]^2}{\sigma_i^2} \qquad (8)$$

(53) Freed, J. H. *J. Chem. Phys.* **1978**, *68*, 4034−4037.

Table 1. Line Width Parameters and Residual Norm χ^2 from Least-Squares Simulations of the Central 10 G Portion of 16-DS X-Band EPR Spectrum of DMPC Sample (pH 9.5) Containing None or 20 MM of Gd-DOTAP[a]
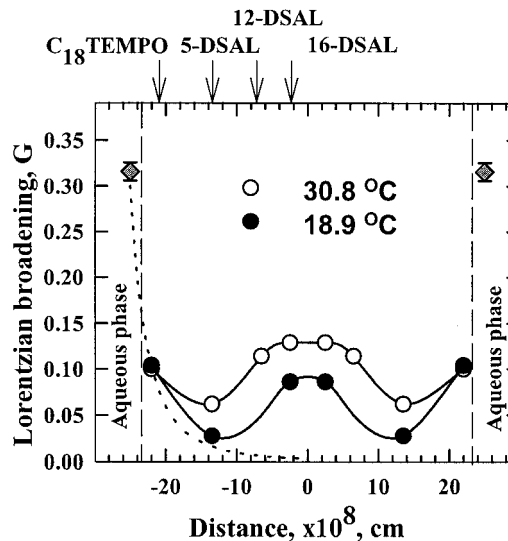
fit	sample	Gaussian, G	Lorentzian, G	$V(\omega)$, G	χ^2
1	0 mM Gd-DOTAP	0.557 ± 0.003	0.970 ± 0.003	0	1.4
2	20 mM Gd-DOTAP	0.557	1.189 ± 0.003	0	21.9
3	20 mM Gd-DOTAP	0.477 ± 0.006	1.276 ± 0.009	0	10.0
4	20 mM Gd-DOTAP	0.557	0.970	0.047 ± 0.003	8.2

[a] The fitting was carried out using different broadening models as discussed in the text.

to be the same for all data points $F(B_i)$, $N = 2000$ was the number of data points, and M was the number of adjustable parameters. This fit gave the width of Lorentzian and Gaussian components of the EPR spectrum from the control sample (Table 1, fit 1).

The EPR spectrum of the membrane sample containing 20 mM Gd-DOTAP was simulated in a few different ways (Table 1, fits 2−4). Initially, a Lorentzian broadening model was assumed and the Gaussian width was set as for the control sample. The residual norm for this fit (Table 1, fit 2) was substantially higher ($\chi^2 = 21.9$) than that for the fit 1 ($\chi^2 = 1.4$). The Gaussian width then was adjusted, and the fit was further improved (fit 3, $\chi^2 = 10.0$). However, a decrease in the Gaussian width from 0.557 ± 0.003 to 0.477 ± 0.006 cannot be explained by either spin exchange or dipole−dipole interaction with Gd-DOTAP; it is most likely to be a result of an incorrect fitting model. The observed trend of decreasing Gaussian and increasing Lorentzian components of the line suggests that the wings of the spectrum are broader than the Lorentzian function. Last, a non-Lorentzian broadening model with $V(a, \omega)$ as defined in eqs 6 and 7 was tried. Both Gaussian and Lorentzian widths were kept at the best-fit values as for the control sample. The residual norm (fit 4, Table 1) further improved to $\chi^2 = 8.2$. Although the last model with non-Lorentzian broadening gave the best fit for the 16-DS/20 mM Gd-DOTAP, the appearance of the relaxation mechanism given by eq 6 still remains quite speculative and more experimental and theoretical studies seem to be necessary. A combined effect of the spin exchange and the dipolar interaction similar to that recently discussed by Galeev and Salikhov[55] should be also considered. A better and a more rigorous approach for calculating motionally averaged spin-label spectra in the presence of a paramagnetic ion would be to solve a stochastic Liouville equation using methods discussed in refs 45 and 46. However, these extended investigations are beyond the scope of this report. Although we cannot give an unambiguous interpretation of the observed line broadening effects at this moment, the dipole−dipole interaction, which is partially averaged by translational diffusion and random spin reorientations, is likely to dominate the electronic spin-label relaxation. The broadening of CW EPR spectra of the spin-labeled DMPC membrane by the presence of Gd-DOTAP was clearly observed and can be reasonably well approximated by either one of the broadening functions (Lorentzian and non-Lorentzian) at concentrations below 10 mM. The magnitude of these effects can be accurately measured by our fitting method and has been analyzed to point to a probable location of the paramagnetic agent within the bilayer.

Broadening effects observed for all membrane labels in the presence of 10 mM Gd-DOTAP were moderately small, and the difference in χ^2 between two broadening models was smaller than that for higher concentrations of Gd-DOTAP (20 mM,

(54) Sachse, J.-H.; King, M. D.; Marsch, D. *J. Magn. Reson.* **1987**, *71*, 385−404.

(55) Galeev, R. T.; Salikhov, K. M. *Chem Phys. Rep.* **1996**, *15*, 359−375.

Figure 7. Profiles of Lorentzian broadening parameter $\delta(\Delta B^{L}_{p-p})$ caused by 10 mM of Gd-DOTAP across the DMPC membrane (pH = 9.5) for two temperatures, below (18.9 °C) and above (30.8 °C) the main phase transition. Approximate location of spin labels in the membrane shown by arrows (DSAL = doxylstearic acid label). Parameter $\delta(\Delta B^{L}_{p-p})$ for the aqueous phase measured with nitroxide tempo-choline is shown as a diamond. Variation of this parameter with the temperature was within the error bars shown. Variations of $\delta(\Delta B^{L}_{p-p})$ for locations are within the size of the symbols. Approximate location of aqueous phase is given by dashed lines. Dotted line shows theoretical $1/r^3$ dependence of line broadening caused by dipole−dipole interaction assuming paramagnetic metal ion to be localized only at the lipid−water interface (see ref 21).

Table 1). Moreover, it was observed that for the 10−20 mM Gd-DOTAP concentration range, the values of the broadening parameters obtained with these two models were approximately proportional. Therefore, either of the broadening parameters can be used to quantify the Gd-DOTAP effects; the Lorentzian broadening model that is more accepted in the literature has been chosen.

Data obtained for several doxyl stearic acid spin labels at temperatures below and above the main phase transition are summarized in Figure 7, which shows the dependence of Lorentzian peak-to-peak broadening caused by 10 mM of Gd-DOTAP upon the distance from the center of the bilayer. The dotted line shows a theoretical $1/r^3$ dependence of line broadening caused by a dipole−dipole interaction if one assumes that the paramagnetic metal ion is localized only at the lipid−water interface.[23] The shape of the profile clearly shows a maximum of the broadening in the bilayer center, indicating a preferred location for Gd-DOTAP there. This is in good agreement with the results of oxygen permeability experiments, which also showed a maximum effect close to the center of the bilayer.

In contrast, we observed no measurable broadening effects upon addition of 10 mM Gd-EOB-DTPA. This confirms our conclusion of the previous section that at the concentrations used, partitioning of Gd-EOB-DTPA is negligible and that this
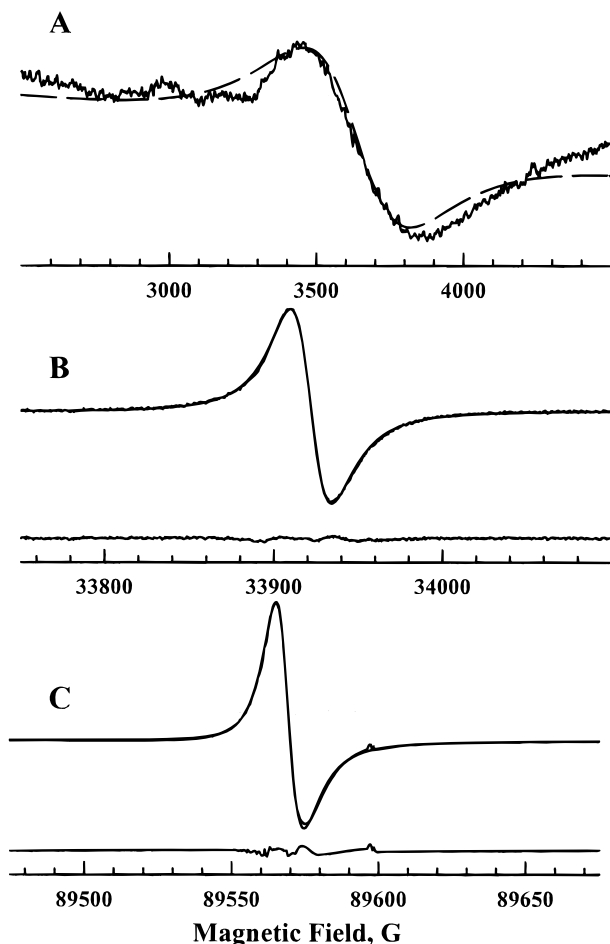
Figure 8. Experimental EPR spectra of 10 mM aqueous solutions of Gd-DOTAP (pH 5.6) at multiple frequencies superimposed with the best fits to Lorentzian lines shape: (A) 9.5 GHz, the best fit shown as a dashed line; Lorentzian peak-to-peak line width $\Delta B^L_{p-p} \approx 400$ G; (B) 94.3 GHz, residual, difference between experimental and simulated spectra, shown at the bottom, $\Delta B^L_{p-p} = 24.6 \pm 0.1$ G; (C) 249 GHz, residual shown at the bottom, $\Delta B^L_{p-p} = 9.3 \pm 0.1$ G. Some small deviations between experiment and fit are likely caused by some small shifting of the resonator frequency during the experiment.

contrast agent does not distort the local order in the phospholipid bilayer. Thus, mechanisms other than diffusion through the phospholipids might be responsible for the transport of Gd-EOB-DTPA through the phospholipid membranes.

Multifrequency and High-Field EPR of Gd³⁺ Complexes. Compared to other lanthanides, Gd^{3+} exhibits a high sensitivity of magnetic parameters to the crystal field. Changes in EPR line width of Gd^{3+} with viscosity-to-temperature ratio (η/T) and upon binding with bovine serum albumin (BSA) have been reported some time ago,[19,27] and it has been speculated that Gd^{3+} could be a useful biological EPR probe to report on local environments.[20] However, low spectral sensitivity, broad line shapes which are poorly understood, and low spectral resolution of X-band EPR for Gd^{3+} spectra made implementation of this idea complicated. Many of these difficulties can be overcome by employing EPR at higher than X-band microwave frequencies.

We have obtained EPR spectra of 10 mM aqueous solutions of Gd-DOTAP (unbuffered, pH $\approx$ 5.6) and Gd-EOB-DTPA at multiple frequencies ranging from 9.5 to 249 GHz (Figure 8) and observed a progressive decrease in EPR line width with increasing microwave frequency. For Gd-DOTAP, the peak-to-peak line width decreases from $\Delta B_{p-p} \approx 400$ G at 9.5 GHz to 24.6 $\pm$ 0.1 G at 94.3 GHz and 9.3 $\pm$ 0.1 G at 249 GHz.
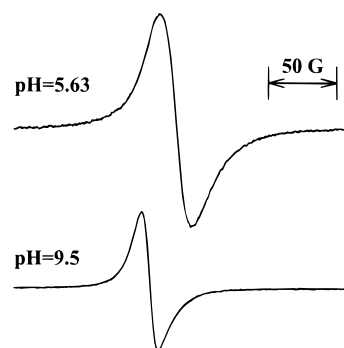

Figure 9. W-band (94.3 GHz) room-temperature EPR spectra of 2 mM Gd-DOTAP aqueous solution at pH 5.6 and 9.5.

Similar decreases were observed for Gd-EOB-DTPA: from $\Delta B_{p-p} \approx 560$ G at 9.5 GHz to about 63 G at 34 GHz to 19.3 $\pm$ 0.1 G at 94.3 GHz. This observation is in qualitative agreement with data reported for other Gd^{3+} compounds studied at multiple EPR frequencies (3, 9.5, 35, and 150 GHz,[29]). The shape of the X-band (9.5 GHz) EPR spectrum of Gd-DOTAP (Figure 8A) cannot be described as Lorentzian, while the EPR spectra at 35 GHz and higher are well approximated by Lorentzian functions (Figure 8B and C), thus simplifying the data analysis. Some asymmetry of the spectra, especially noticeable at 94.3 and 249 GHz, is caused by an admixture of dispersion into the signal, a typical occurrence in HF EPR experiments with single-channel detection.[13,31,37] To correct for this effect, the fitting involved a Lorentzian function derived for an arbitrary mixture of absorption and dispersion signals[37] and the phase was independently adjusted during the Levenberg–Marquardt optimization.

Sensitivity of HF EPR spectra of Gd^{3+} complexes to the properties of the solvent is demonstrated by a pH dependence of the width and of the apparent g-factor of the 2 mM Gd-DOTAP EPR spectrum at 94.3 GHz (Figure 9). With increasing pH from ∼5.6 (unbuffered aqueous solution) to 9.5 (borate buffer), the Lorentzian peak-to-peak line width decreased from 23.19 $\pm$ 0.05 G to 14.58 $\pm$ 0.05 G and the apparent isotropic g-factor, g_{eff}, increased from 1.990 32 to 1.991 06. (The estimated accuracy of all g-factors measured here from W-band data is at least 3 $\times$ 10⁻⁵ or better.) The distance between zero crossing points of the W-band EPR signals from Gd-DOTAP solutions at two different pH values, 5.6 and 9.5, was ∼12.5 G.

The sensitivity of Gd-DOTAP 94.3 GHz EPR spectra to the solute was further utilized to observe the interaction of this complex with the DMPC bilayer. Figure 10 shows an experimental 94.3 GHz EPR spectrum from 5 mM Gd-DOTAP added to a 5.5% multilamellar DMPC aqueous dispersion (pH 9.5, $T = 31$ °C). The spectrum can be very well fitted as a superposition of two Lorentzian lines with different g-factors and line widths; the phase shift for two signals was assumed to be the same. Comparison of the width of the narrow line ($\Delta B^L_{p-p}(1) = 13.39 \pm 0.03$ G) and its g-factor ($g_{eff} = 1.991\ 02$) with the signal observed in solution at pH 9.5 shows that the narrow signal originates from Gd-DOTAP in the aqueous phase. The broader line ($\Delta B^L_{p-p}(2) = 28.0 \pm 0.1$ G) with a smaller g-factor ($g_{eff} = 1.990\ 30$) is assigned to the Gd^{3+} complex partitioned or interacting with the lipid phase of the phospholipid bilayer. The broad signal associated with the lipid phase accounts for 59 $\pm$ 2% of the overall double-integrated intensity. A single-line spectrum was observed at 94.3 GHz for a number of DMPC samples containing various concentrations of Gd-
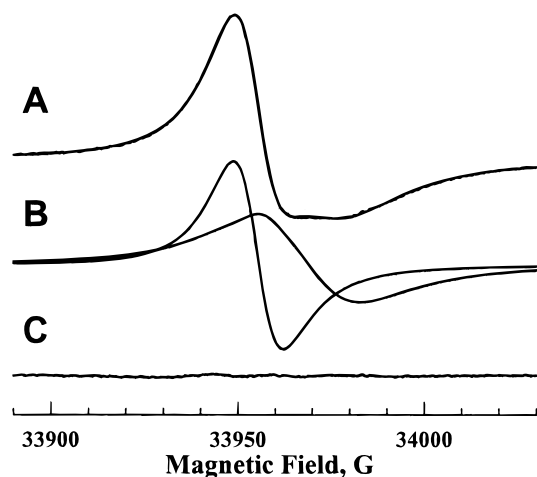
Figure 10. (A) Experimental 94.3 GHz EPR spectrum from Gd-DOTAP added to a 5.5% multilamellar DMPC aqueous dispersion (pH 9.5) to final concentration of 5 mM ($T = 31$ °C). The spectrum can be well fitted as a superposition of two Lorentzian lines with different *g*-factors and line widths (B). The narrow line ($\Delta B^{L}_{p-p}(1) = 13.39 \pm 0.03$ G) is assigned to Gd-DOTAP in aqueous phase at pH 9.5; the broader line ($\Delta B^{L}_{p-p}(2) = 28.0 \pm 0.1$ G), to the Gd^{3+} complex partitioned or interacting with the lipid phase of the bilayer. Spectra C is the residual, the difference between experimental and simulated spectra.

EOB-DTPA. This observation is consistent with the conclusions of our spin-labeling experiments that Gd-EOB-DTPA does not measurably partition into the phospholipid bilayer.

Partitioning of Gd-DOTAP within the phospholipids was further supported by model experiments in which Gd-DOTAP was introduced into a lipid-like environment by mixing oleic acid with a 5 mM aqueous solution of the complex at room temperature and various pH values. The dispersions and micellar solutions (at high pH) so obtained were further separated by a centrifugation, which yielded two phases with a clearly observed interface for all mixtures. The oleic acid phase was collected separately and did show a Gd^{3+} EPR signal. The introduction of Gd-DOTAP into oleic acid from the aqueous solution seems to be a useful model for partitioning of Gd-DOTAP within the phospholipids. This procedure, in principle, might allow the complex to retain some water molecules, at least at the vacant coordination site. Direct observation of a Gd^{3+} EPR signal in a lipid-like solvent demonstrates that Gd-DOTAP possesses sufficient lipophilicity to partition into phospholipid membranes, thus confirming the results of spin-labeling experiments. When Gd-DOTAP is introduced from aqueous solution at a low pH of 5.6, the signal can be well fitted to a Lorentzian function of width $\Delta B^{L}_{p-p} = 26.25 \pm 0.05$ G, which is only slightly narrower than the width of the broader line in the DMPC partitioning experiments. The signal was shifted to higher magnetic field ($g_{eff} = 1.990\ 93$), which is consistent with the direction of the shift observed for the lipid-associated signal. For Gd-DOTAP introduced from aqueous solution at a high pH, 9.5, the W-band spectra show the presence of at least two signals; the *g*-factor of one of the signals, $g_{eff} = 1.990\ 38$, was very close to that observed for the "broad" line in the DMPC partitioning experiment ($g_{eff} = 1.990\ 30$). Overall, the model 94.3 GHz EPR experiments with oleic acid demonstrate that Gd-DOTAP partitions into the lipid-like phase and that the direction of the *g*-factor shift is consistent with that observed in the DMPC-partitioning experiment, further confirming the assignments of the lines.
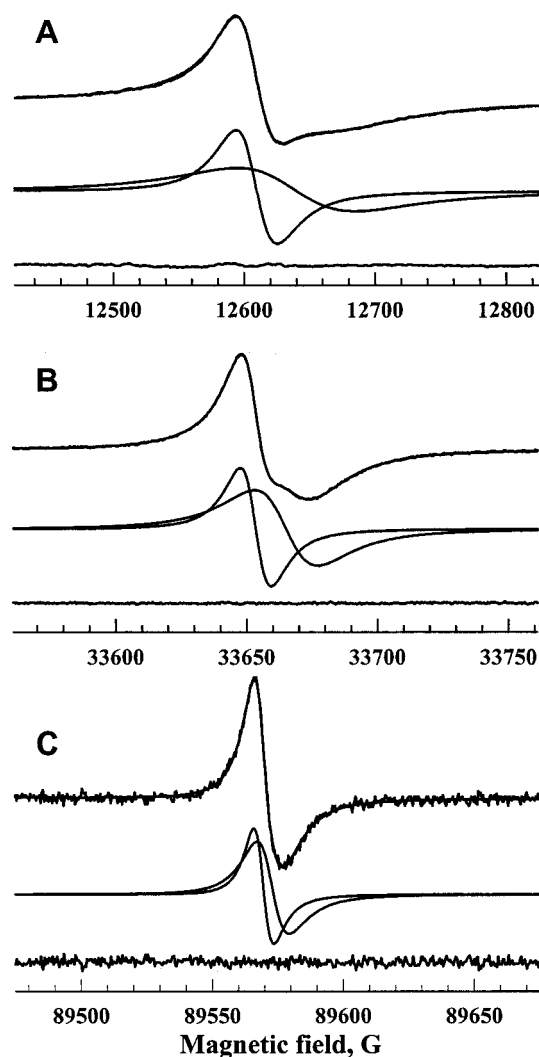
Figure 11. Experimental room-temperature EPR from Gd-DOTAP added to a 5.5% multilamellar DMPC aqueous dispersion (pH 9.5) to 10 mM final concentration at 35 GHz (A), 94.2 GHz (B), and 249 GHz (C). Each spectrum can be well fitted as a superposition of two Lorentzian lines with different widths and *g*-factors. Simulations are presented under the corresponding spectra. Residuals, shown just above the magnetic field scales, demonstrate good agreement between the experimental and simulated spectra. The splitting between the lines decreases with the EPR frequency.

To understand the nature of the apparent *g*-shift for the EPR signal from Gd-DOTAP, partitioned in a phospholipid bilayer, we obtained EPR spectra of Gd-DOTAP in a 5.5% DMPC dispersion (pH 9.5) at two other frequencies, 35 and 249 GHz (Figure 11). A higher concentration of Gd-DOTAP, 10 mM, was chosen to ensure a good signal-to-noise ratio at all EPR frequencies. Although the two signals are less resolved at 249 GHz than at 35 GHz, at both frequencies the spectra from Gd-DOTAP in 5.5% DMPC dispersion can be described with the same model as for the W-band spectrum: a superposition of two Lorentzian lines with different *g*-factors and line widths. At all three EPR frequencies, the signal assigned to lipid-associated Gd-DOTAP is shifted to higher magnetic field. The splitting between the lipid and the aqueous components decreased with the EPR frequency, and this cannot be explained by the polarity effect on the *g*-factor that is typically observed for free radicals;[56,57] for free radicals, the sign of the *g*-shift with polarity is opposite to that observed in our experiments.

Changes in the apparent g-factor of Gd^{3+} EPR signals with magnetic field can be explained by considering the contribution of the zero-field splitting (ZFS) term to the spin Hamiltonian:

$$\mathcal{H} = \mathcal{H}_{Zeeman} + \mathcal{H}_{ZFS} = \beta \cdot \boldsymbol{B} \cdot \boldsymbol{g} \cdot \boldsymbol{S} + \boldsymbol{S} \cdot \boldsymbol{D}_{ZFS} \cdot \boldsymbol{S} = \beta \cdot \boldsymbol{B} \cdot \boldsymbol{g} \cdot \boldsymbol{S} +$$
$$D(S_z^2 - \tfrac{1}{3}S^2) + E(S_x^2 - S_y^2) + \tfrac{1}{3}S^2(D_x + D_y + D_z) \quad (9)$$

where $\mathcal{H}_{Zeeman}$ and $\mathcal{H}_{ZFS}$ are electron Zeeman and ZFS parts of the Hamiltonian, $\boldsymbol{D}_{ZFS}$ is the zero field splitting tensor, $\boldsymbol{B}$ is the magnetic field vector, and $\boldsymbol{S}$ is the electron spin operator. Ordinarily, $D_x + D_y + D_z = 0$. With an increase in the magnetic field B, the relative contribution of the ZFS term to the spin Hamiltonian becomes smaller than that of the electronic Zeeman term. For aqueous solutions of several Gd^{3+} complexes, the Δ^2 is estimated of the order of 1 GHz.[30] Thus, at frequencies of Q-band EPR (35 GHz) and higher, $\mathcal{H}_{ZFS}$ can be treated as a small perturbation to the Hamiltonian, and it will cause a shift of the resonance field of order $D^2/g\beta B$ depending upon spin orientation in the magnetic field.[28,65] For solution spectra, this shift is averaged by rotational motion. The shape of such a spectrum is determined by distribution of the electron spins over the states which, for magnetically anisotropic systems, is affected by angular distribution of the species, and rates of spin exchange between the states. It has been shown, based on the solution to modified Bloch equations, that the first moment of the spectrum is determined by the spin distribution over the states alone and is independent of the exchange frequency between the states.[66] This result was obtained under the assumption that the molecular motion neither changes the spin precession phase nor perturbs the states. Under these conditions, the resonance field at which the first moment of the spectrum is zero is independent of the rate of motional averaging as long as the overall angular distribution of the spins, a distribution which remains isotropic because of the random orientation of Gd complexes remains the same. If these assumptions are valid for the Gd^{3+} complexes of interest in solution, then the observed shift of the resonance field can be calculated by averaging the resonance position over all angular orientations. For these calculations, we have started with an explicit expression of the transition energy for the spin Hamiltonian (eq 9) that is valid to the third order of perturbation.[67,68] For the allowed $|^1/_2\rangle \leftrightarrow |-^1/_2\rangle$ transition, this energy is given by

(56) Kawamura, T.; Matsunami, S.; Yonezawa, T. *Bull. Chem. Soc. Jpn.* **1967**, *40*, 1111−1115.

(57) Earle, K. A.; Moscicki, J. K.; Ge, M.; Budil, D. E.; Freed, J. H. *Biophys. J.* **1994**, *66*, 1213−1221.

(58) Kowall, T.; Foglia, F.; Helm, L.; Merbach, A. E. *J. Phys. Chem.* **1996**, *99*, 13078−13087.

(59) Chen, J. W.; Auteri, F. P.; Budil, D. E.; Belford, R. L.; Clarkson, R. B. *J. Phys. Chem.* **1994**, *98*, 13452−13459.

(60) Chen, J. W.; Clarkson, R. B.; Belford, R. L. *J. Phys. Chem.* **1996**, *100*, 8093−8100.

(61) Wiener, E. C.; Auteri, F. P.; Chen. J. W.; Brechbiel, M. W.; Gansow, O. A.; Schneider, D. S.; Belford, R. L.; Clarkson, R. B.; Lauterbur, P. C. *J. Am. Chem. Soc.* **1996**, *100*, 8093−8100.

(62) Rubinstein, M.; Baram, A.; Luz, Z. *Mol. Phys.* **1971**, *20*, 67−80.

(63) Alpert, Y.; Couder, Y.; Tuchendler, J.; Thomé, H. *Biochim. Biophys. Acta* **1973**, *322*, 34−37.
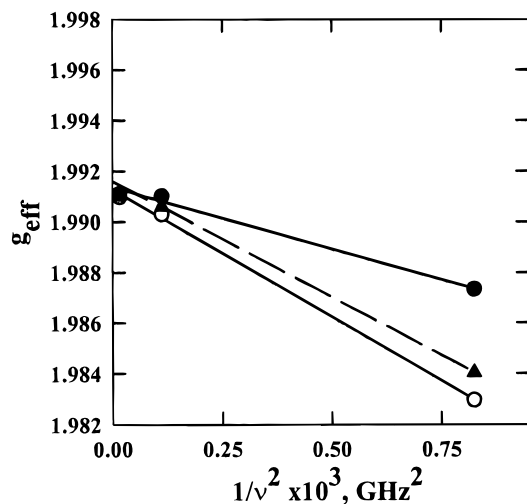
(64) Gaffney, B. J.; Silverstone, H. J. In *Biological Magnetic Resonance*; Berliner, L. J., Reuben, J., Eds.; Plenum Press: NY, 1993; pp 1−58.

(65) Weil, J. A. *J. Magn. Reson.* **1975**, *18*, 113−116.

(66) Grinberg, O. Ya.; Dubinskiî, A. A.; Poluektov, O. G.; Lebedev, Ya. S. *Sov. J. Chem. Phys. (Engl. Transl.)* **1990**, *6*, 2685−2704.

(67) Meirovich, E.; Poupko, R. *J. Phys. Chem.* **1978**, *82*, 1920−1925.

(68) Lynch, W. B.; Boorse, R. S.; Freed, J. H. *J. Am. Chem. Soc.* **1993**, *115*, 10909−10915.

$$E_{1/2} - E_{-1/2} = h\nu = g\beta B - \frac{2B_+ 2B_- G}{\omega_0} + \frac{C_+ C_- G}{\omega_0} \quad (10)$$

where

$$B_{\pm} = {}^D/_4\{-\sin 2\theta + \eta \sin 2\theta \cos 2\varphi \pm i2\eta \sin \theta \sin 2\varphi\} \quad (11)$$

$$C_{\pm} = {}^D/_4\{-\sin^2 \theta + \eta(\cos^2 \theta + 1)\cos 2\varphi \pm$$
$$i2\eta \cos \theta \sin 2\varphi\}$$

$$\omega_0 = g\beta B_0$$

$$G = 4S(S + 1) - 3$$

The shift of the resonance field ΔB caused by the ZFS term in the spin Hamiltonian can be expressed as a function of the polar angles θ and φ:

$$\Delta B(\theta,\varphi) = \frac{G}{g\beta\omega_0}(C_+C_- - 2B_+B_-) \quad (12)$$

Averaging $\Delta B(\theta, \varphi)$ over all orientations gives

$$\langle \Delta B \rangle_{\theta,\varphi} = \frac{\int_0^{2\pi} \int_0^{\pi} \Delta B(\theta,\varphi) \sin \theta \, d\theta \, d\varphi}{\int_0^{2\pi} \int_0^{\pi} \sin \theta \, d\theta \, d\varphi} =$$
$$\frac{D^2}{30 \, g\beta\omega_0}(4S(S + 1) - 3)(1 + 3\eta^2) \quad (13)$$

where $\eta = E/D$. For Gd^{3+} ion, $S = {}^7/_2$, so from eq 13 the effective isotropic g-factor can be derived as:

$$g_{eff} = g\left(1 - \frac{2D^2(1 + 3\eta^2)}{\omega_0^2}\right) \quad (14)$$

Equation 14 can be recast in terms of the squared ZFS matrix $\Delta^2 = (D_x^2 + D_y^2 + D_z^2)/\hbar$:

$$g_{eff} = g\left(1 - \frac{3\Delta^2}{(2\pi\nu)^2}\right) \quad (15)$$

Thus, if two species have the same g-factors but different ZFS parameters, the difference in g_{eff} between the two signals decreases with the increase of resonance frequency ν.

Figure 12 shows a plot of the apparent g-factors versus $1/\nu^2$ for the aqueous and the lipid signals of Gd-DOTAP in a 5.5% DMPC dispersion as measured at 35, 94, and 249 GHz, together with the results of linear regression (eq 11). The estimated ZFS parameter Δ is 8.1 rad GHz for the lipid Gd-DOTAP phase and 5.65 rad GHz for the aqueous Gd-DOTAP phase (pH 9.5). Figure 12 also shows that intercept with the g-factor axis occurs at $g = 1.9914$ for the aqueous and at $g = 1.9913$ for the lipid Gd-DOTAP EPR signals. The difference in these g-factors is within the error of calibrating magnetic field between different spectrometers. We speculate that effect of the media on the

Figure 12. Apparent *g*-factors (g_{eff}) vs $1/\nu^2$ as measured at 35, 95, and 250 GHz and the results of linear regression (eq 11) for the aqueous (filled circles) and the lipid (open circles) EPR signals observed in 5.5% DMPC aqueous dispersion (pH 9.5) after addition of Gd-DOTAP to a 10 mM concentration. Filled triangles correspond to apparent *g*-factors as measured at 35 and 95 GHz for unbuffered 4 mM aqueous solution of Gd-EOB-DTPA; linear regression is shown as a dotted line. The estimated ZFS parameter Δ is 8.1 rad GHz for the lipid and 5.65 rad GHz for the aqueous Gd-DOTAP phase in DMPC membrane and 7.8 rad GHz for aqueous Gd-EOB-DTPA.

g-factor of an s-state ion is rather small, particularly for Gd^{3+} whose paramagnetic inner 4f orbitals are well shielded by outer 5s and 5p electrons. Measurements at EPR frequencies much higher than 95 GHz are definitely needed to further clarify this issue.

For unbuffered aqueous solution of another PCA studied here—Gd-EOB-DTPA—no 249 GHz spectra were acquired, so we can only roughly estimate the ZFS parameter as $\Delta \approx 7.8$ rad GHz from 35 and 94 GHz data (shown as a dashed line in Figure 12). Again, the *g*-factor axis intercept ($\sim$1.9916) is close to that for Gd-DOTAP.

While there are no estimates for ZFS parameters of Gd-DOTAP and Gd-EOB-DTPA in the literature, the values obtained in this work are close to those previously reported for some other Gd^{3+} complexes.[29,30] The values we measure here from the multifrequency solution EPR spectra can be compared with more routine measurements of ZFS parameters from simulation of rigid-limit EPR spectra of frozen solutions. For example, simulation of the rigid-limit 94 GHz EPR spectrum from unbuffered 1 mM Gd-DOTAP/glycerol mixture (50% glycerol by volume, $T = 180$ K) with the program PIP[42] gave $E \approx 600$ MHz and $D \approx 1800$ MHz, corresponding to $\Delta \approx 10.7$ rad GHz. This value is close to $\Delta \approx 8.1$ rad GHz which we measured from frequency dependence of g_{eff} for unbuffered Gd-DOTAP aqueous solution (pH $\approx$ 5.6) at room temperature. Magnetic parameters of this PCA in a frozen solution at a low temperature and at a more physiologically relevant conditions—liquid solution at room temperature—are not necessarily the same. This PCA in a frozen solution at low temperature does not necessarily have exactly the same magnetic parameters as in liquid solution at a room temperature, which is more physiologically relevant. This raises a further question, i.e., whether ZFS parameters are affected by temperature and, if so, to what extent, that needs to be answered.

Multifrequency EPR data summarized in Figure 12 show that the ZFS parameter Δ is larger for Gd-DOTAP associated with a DMPC bilayer than for Gd-DOTAP in the aqueous phase at high pH (9.5 in this experiment). This effect is opposite to the decrease in the ZFS parameter Δ reported for Gd^{3+} ion upon binding to bovine serum albumin, as derived from interpretation of the variable temperature EPR line width data at X- and Q-band.[27]

Any determination of ZFS parameters from EPR line width measurements or in combination with ^{17}O and magnetic resonance dispersion (NMRD) data implies an application of electron spin relaxation theory under a specific model. For Gd^{3+} complexes, the main contribution to the electronic relaxation is considered to be due to the ZFS,[30] which may be modulated by the motion of the water molecules in the first hydration shell of the complex or by changes of the distortion axis.[58] Other relaxation mechanisms such as spin-rotation,[59–61] concentration broadening,[29] and anisotropic *g*-factor[62] also contribute to the line width, and some of these effects are field dependent. As a result, the magnitude of the ZFS is coupled to a number of parameters of the relaxation model. It is possible that the same relaxation model does not apply to paramagnetic ions in both aqueous solution and a phospholipid bilayer. The method of estimation of ZFS from the frequency dependence of the apparent *g*-factor described here seems to be less model-dependent. Determination of the ZFS from multifrequency EPR data is not novel in the literature, but so far it has been demonstrated only for rigid-limit spectra[63,64] and not for solution spectra.

Conclusions

The use of spin-labeling EPR methods to study lipid−contrast agent interactions by monitoring changes in the structural organization of the membrane has been demonstrated. The changes in the local oxygen permeability coefficient across the bilayer point to a possible location of a lipophilic Gd-DOTAP complex close to the central portion of the membrane when the bilayer is in the fluid phase. These results agree with the magnitude of spin-label spectra broadening in the presence of Gd-DOTAP. The broadening was found to be maximal for the spin labels located at positions 12 and 16 of the acyl chain, confirming the location of this PCA in the bilayer center.

These spin-labeling experiments have shown that two lipophilic contrast agents interact with the phospholipid bilayer very differently. The Gd-DOTAP complex penetrates and partitions within the lipid phase of the bilayer, while the presence of Gd-EOB-DTPA within bilayer cannot be definitely established by EPR methods described here. Thus, a mechanism other than nonspecific diffusion may be responsible for intracellular transport of Gd-EOB-DTPA.

The presence of Gd-DOTAP within the phospholipid membrane was additionally confirmed with 95 GHz EPR. Measurements at 35 and 95 GHz resolved the EPR signals from Gd-DOTAP complexes partitioned between the aqueous and the phospholipid phases of the bilayer and determined the partition coefficient.

The EPR experiments at multiple high frequencies (35, 94, and 249 GHz) show that the observed spectral resolution at the higher frequencies arises from line narrowing due to a decreased relative contribution of ZFS in the spin Hamiltonian at higher magnetic fields and that the resonance signal shifts due to ZFS effects. Analysis of the frequency dependence of apparent *g*-factors for aqueous and lipid signals yields an estimate of the ZFS parameters of Gd^{3+} complexes in the physiologically relevant liquid environment. It is demonstrated that the ZFS increases when this PCA partitions within the membrane. This strengthens an existing opinion that interactions of Gd PCAs

Smirnova et al.

with a biological environment may affect the ZFS parameter so as to modify proton relaxation enhancement by PCA.

JA973427N